

## Supplementary Information

### Bioactive Silver Phosphate/Polyindole Nanocomposites

Soumik Podder, Samrat Paul, Piyali Basak, Bowen Xie, Nigel J. Fullwood, Sara J. Baldock, Ying Yang, John G. Hardy\* and Chandan K. Ghosh\*

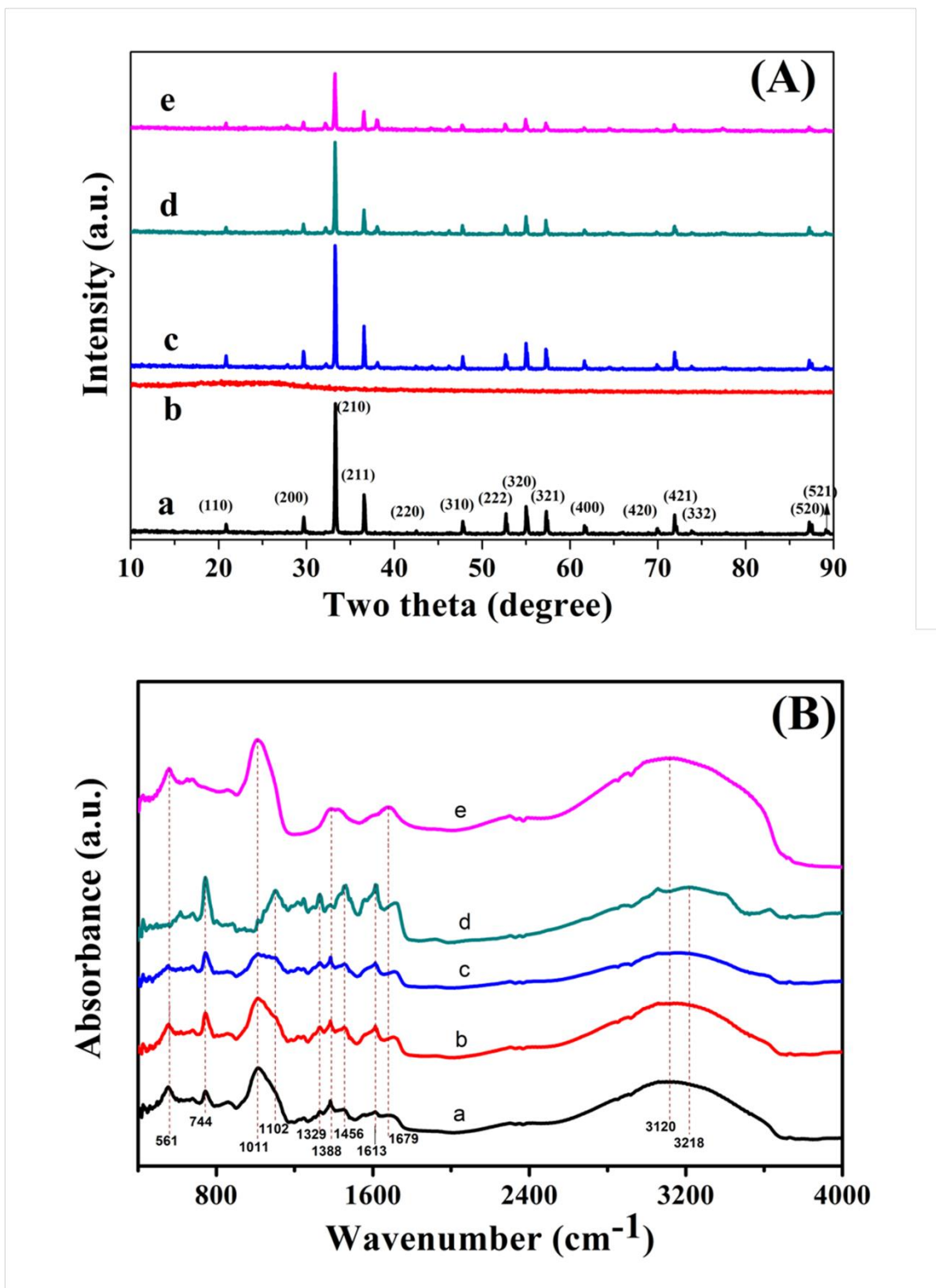
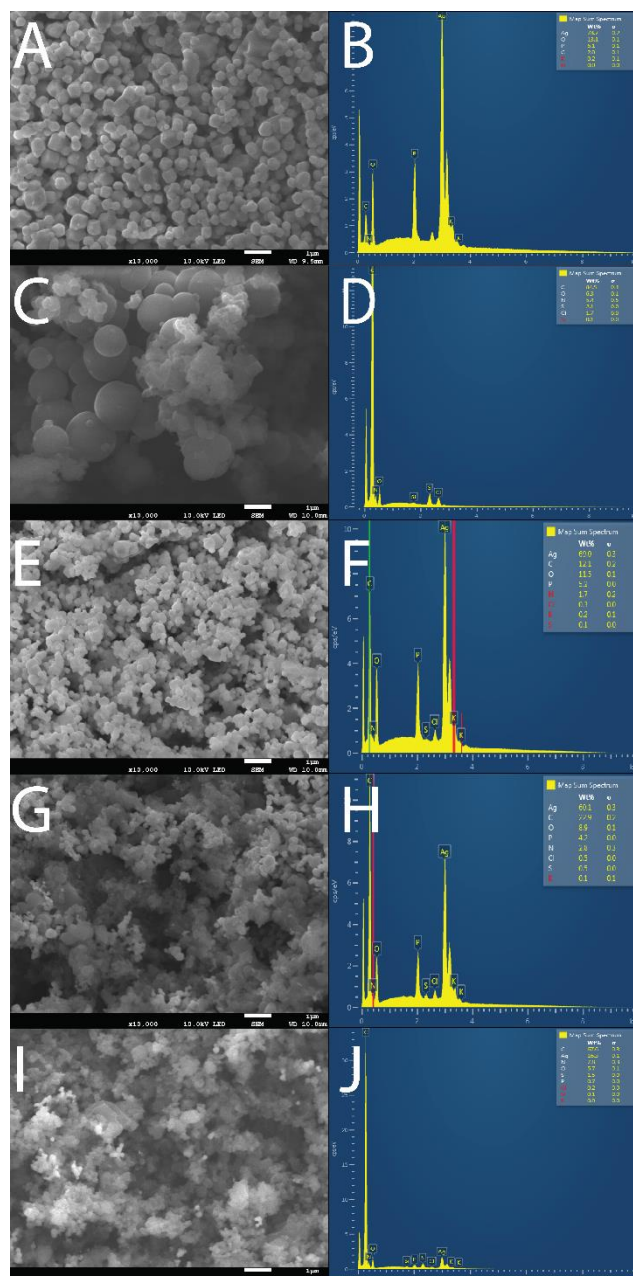
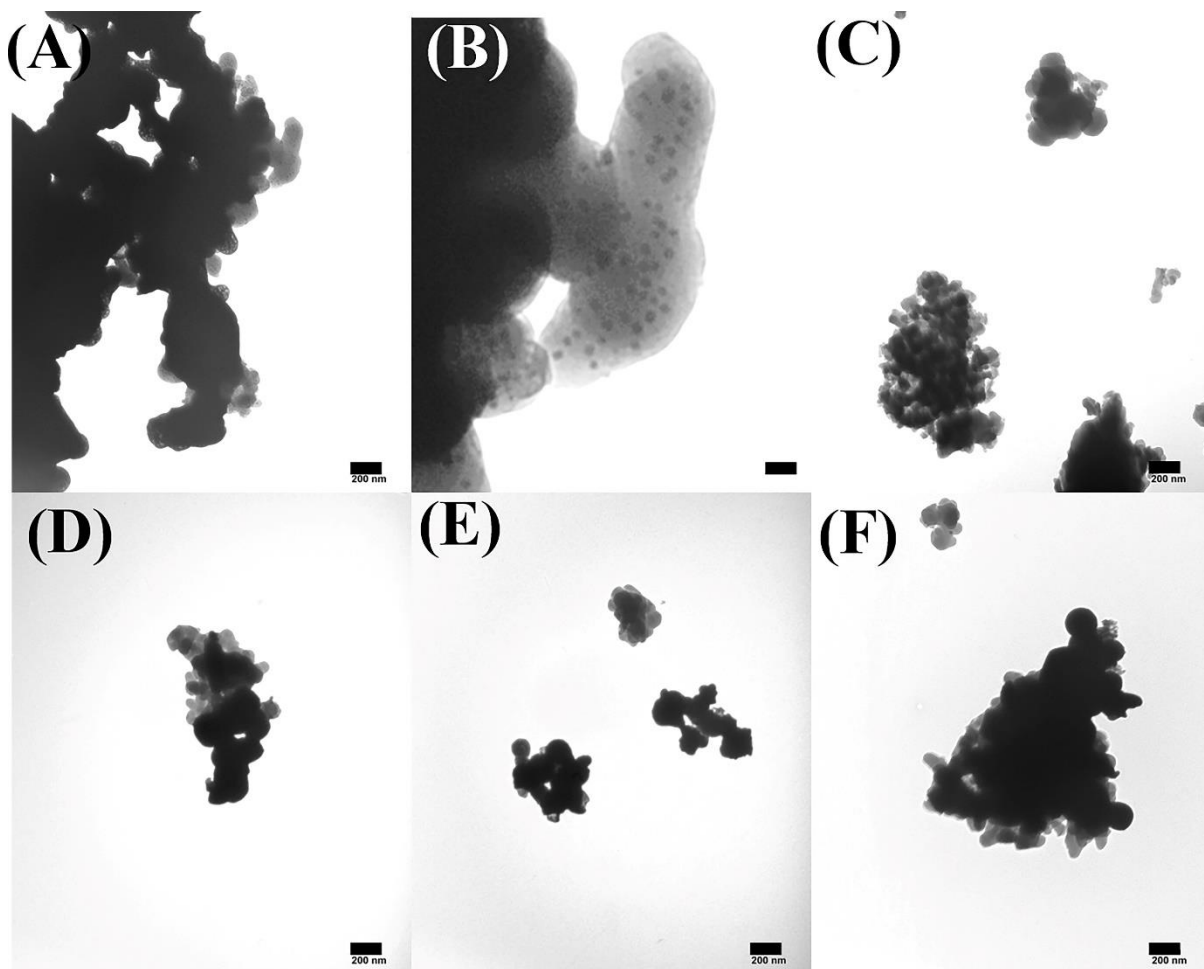


Fig S1. (A) XRD pattern of a.  $\text{Ag}_3\text{PO}_4$ , b.  $\text{PIn}_0$ , c.  $\text{PIn}_1$ , d.  $\text{PIn}_2$ , e.  $\text{PIn}_3$ ; (B) FTIR spectra of a.

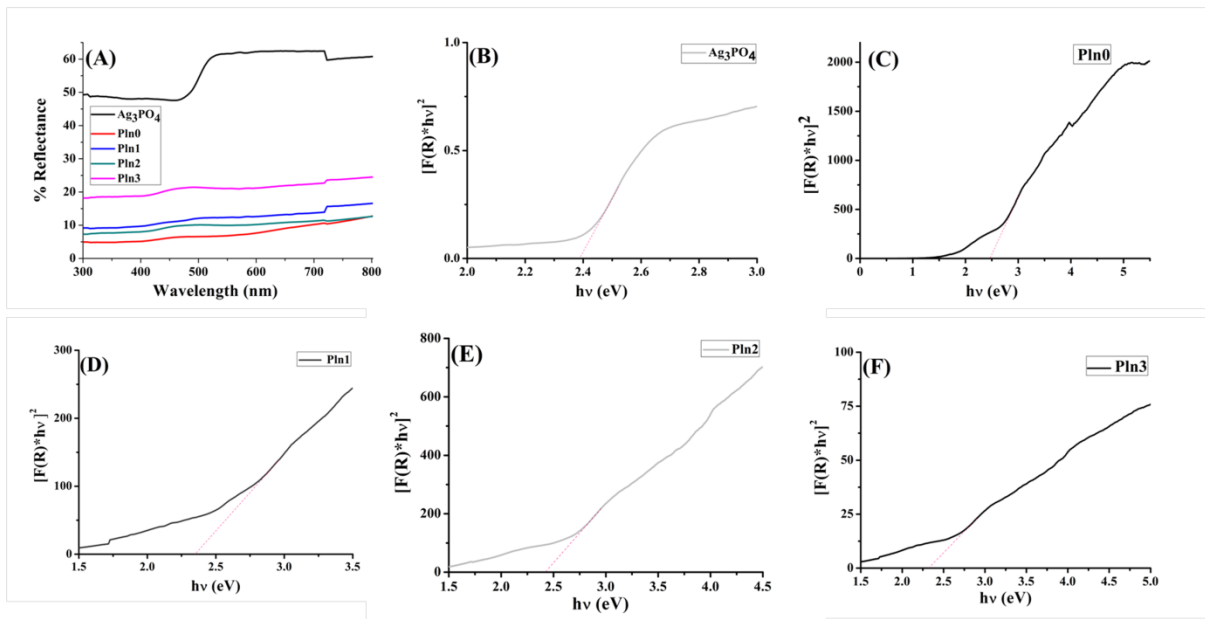
$\text{PIn}_1$ , b.  $\text{PIn}_2$ , c.  $\text{PIn}_3$ , d.  $\text{PIn}_0$  and e.  $\text{Ag}_3\text{PO}_4$ .



**Fig S2.** SEM images and EDX spectra. **A&B)** Ag<sub>3</sub>PO<sub>4</sub>. **C&D)** Pln0. **E&F)** Pln1. **G&H)** Pln2. **I&J)** Pln3.**A/B/C/D/E)** SEM images; scale bars represent 1 μm. **B/D/F/H/I)** EDX spectra. **B)** Ag (78.7%), O (13.1%), P (6.1%), C (2.0%), K (0.2%), N (0.0%). **D)** C (84.5%), O (6.3%), N (5.4%), S (2.1%), Cl (1.7%), Si (0.1%). **F)** Ag (69.0%), C (12.1%), O (11.5%), P (5.2%), N (1.7%), Cl (0.3%), K (0.2%), S (0.1%).**H)** Ag (60.1%), C (22.9%), O (8.9%), P (4.2%), N (2.8%), Cl (0.5%), S (0.5%), K (0.1%).**J)** C (67.6%), Ag (16.3%), N (7.8%), O (5.7%), S (1.5%), P (0.7%), Cl (0.2%), Si (0.1%), K (0.0%).



**Fig S3.**(A)-(F) TEM micrographs of  $\text{Ag}_3\text{PO}_4$  (A,B), PIn0 (C), PIn1 (D), PIn2 (E) and PIn3 (F) respectively. The TEM results largely correlate with the SEM images showing small agglomerates of mostly spherical particles with some angular and oblate structures visible. Figure S3 (B) shows that the  $\text{Ag}_3\text{PO}_4$  particles are not homogeneous but contain  $\sim 10\text{nm}$  sized inclusions, visible at high magnification. Scale bars: 200nm (A,C,D,E,F), 30nm (B).



**FigS4.** Optical Characterization of the Composite by Diffused Reflectance Spectroscopy. A) DRS spectra of Ag<sub>3</sub>PO<sub>4</sub>/Pln nanocomposites. B-F) Kubelka-Munk plots. B) Ag<sub>3</sub>PO<sub>4</sub>. C) Pln0. D) Pln1. E) Pln2. F) Pln3.

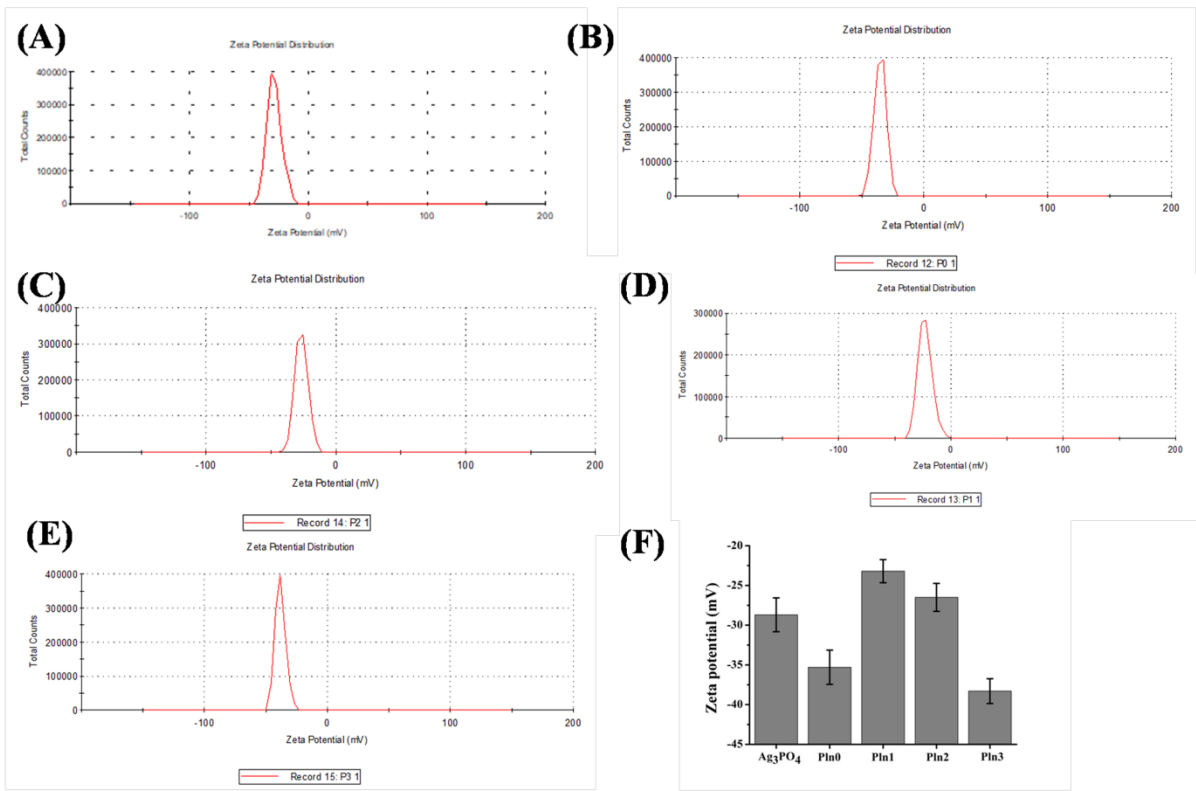


**Fig S5.** Zeta potential studies. A) Ag<sub>3</sub>PO<sub>4</sub>. B) Pln0. C) Pln1. D) Pln2. E) Pln3. F) Zeta potential variation among Ag<sub>3</sub>PO<sub>4</sub>/Pln composites.

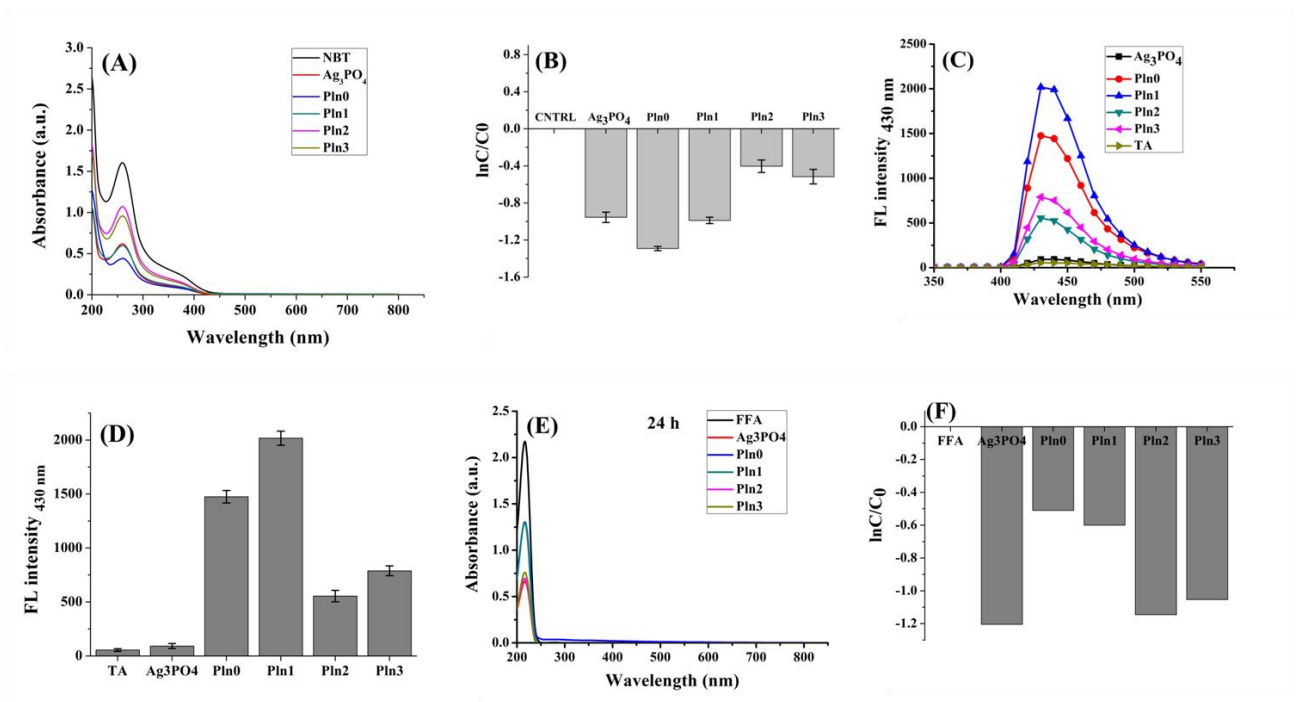


**Fig. S6** In-vitro ROS generation. A) Absorbance spectra of NBT in presence of Ag<sub>3</sub>PO<sub>4</sub>/PIncomposites after 24 h in the dark. B) Degradation of NBT in presence of nanocomposites after 24 h exposure in the dark, NBT is used as control (CNTRL). C) FL spectra of 2-hydroxy terephthalic acid in presence of nanocomposites after 24 h in the dark. D) Comparative ·OH generation from nanocomposites after 24 h in the dark, (E) Absorbance spectra of FFA in presence of Ag<sub>3</sub>PO<sub>4</sub>/PIncomposites after 24 h in the dark. (F) Degradation of FFA in presence of nanocomposites after 24 h exposure in the dark, FFA is used as control (CNTRL).

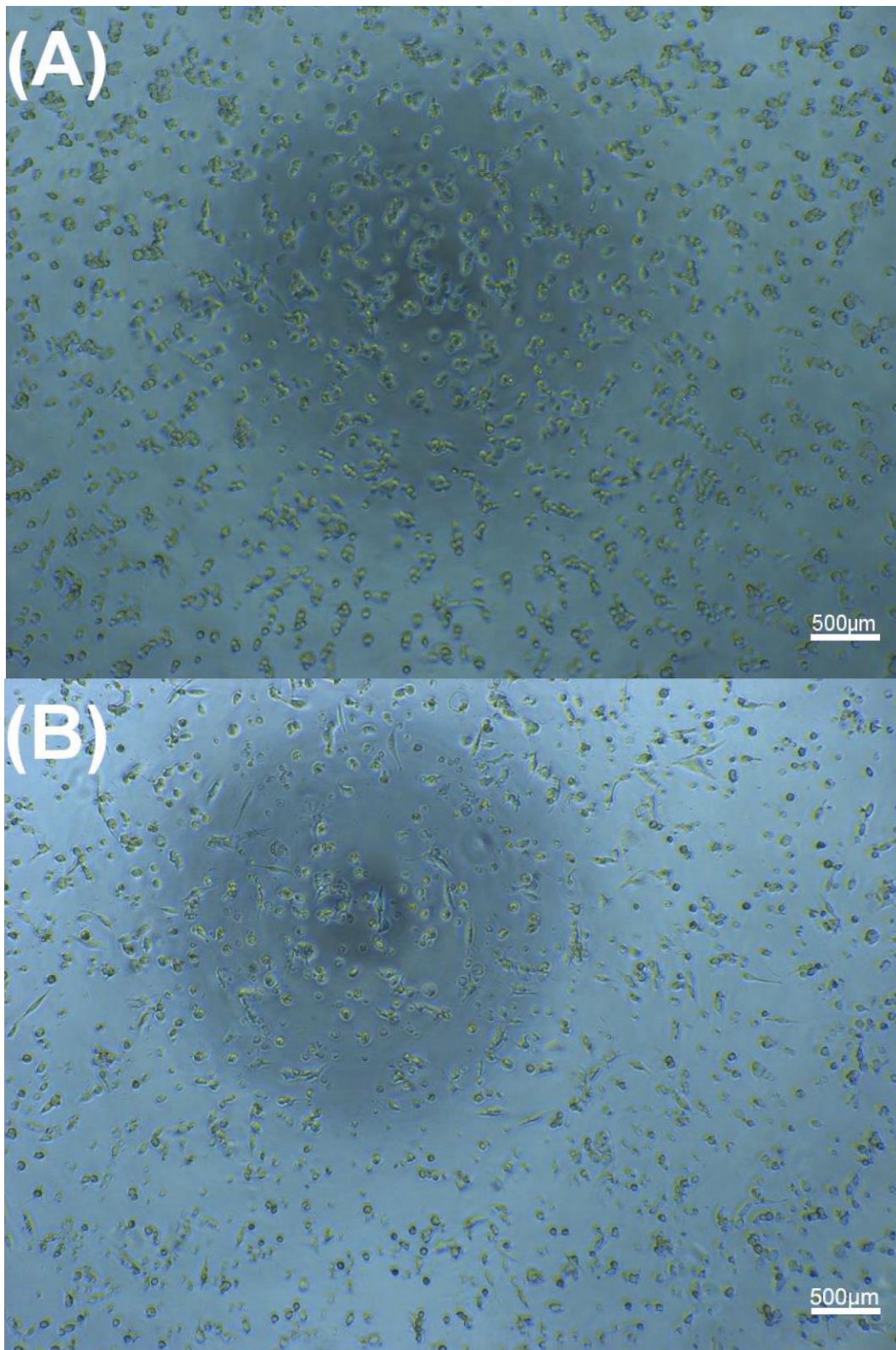


**Fig S7.** Morphology of human monocyte THP-1 derived macrophages. A) before LPS stimulation. B) after LPS treatment.